AIAA SciTech Forum
11–15 & 19–21 January 2021, VIRTUAL EVENT
AIAA Scitech 2021 Forum

10.2514/6.2021-0685

Dark Discharge Streamer Simulations Using a Spectral Deferred Correction Strategy

Nicholas Deak*, Alfredo Duarte †, Fabrizio Bisetti‡
The University of Texas at Austin, Austin, Texas, 78712

Numerical simulations of atmospheric air streamers at 300 K are performed using a one-dimensional model with a local field approximation. Transport equations for electrons and ions, including drift, diffusive, and reactive processes are solved via a spectral deferred correction (MISDC) method, which is used to advance the solution with time steps of size comparable to the drift time scales. A simplified chemistry model based on a quasi-steady state assumption accounting for electron impact ionization, electron-ion and ion-ion recombination, electron attachment, electron detachment, and seed charge generation is employed. An improved set of boundary conditions for the electrons and ions are used to model ion and electron fluxes at the electrode boundaries. In order to test the performance of the algorithm, a suite of steady-state solutions to a boundary value problem are formulated. It is found that for simulations with a strong applied electric field ($E/N \approx 100$ Td), the time step size required for the solution to converge is limited by the electron drift velocity when the electron drift is solved explicitly. The improved boundary conditions are found to produce sharp gradients near the electrodes that require grid resolution finer than what is typically used in streamer modeling (sub-micron grid spacing). This is found to impose severe numerical restrictions given the explicit handling of the advective terms.

I. Nomenclature

n_e	=	electron number density (cm^{-3})
n_k	=	ion number density (cm^{-3})
$\mu_{e,k}$	=	electron and ion mobilities ($cm^2\ V^{-1}\ s^{-1}$)
$\mathcal{D}_{e,k}$	=	electron and ion diffusivities ($cm^2\ s^{-1}$)
Z_k	=	ion charge
$\mathbf{E}$	=	electric field ($V\ cm^{-1}$)
$\dot{\omega}_{e,k}$	=	electron and ion source terms ($cm^{-3}\ s^{-1}$)
ϕ	=	electric potential (V)
e	=	unit charge (C)
ε_0	=	vacuum permitivity ($F\ cm^{-1}$)
ε_r	=	relative permitivity
$\mathbf{A}_{e,k}$	=	electron and ion advective terms ($cm^{-3}\ s^{-1}$)
$\mathbf{D}_{e,k}$	=	electron and ion diffusive terms ($cm^{-3}\ s^{-1}$)
N_i	=	number of ions
N	=	Neutral species number density (cm^{-3})
$\mathbf{U}$	=	state variables
$\mathbf{E}_0$	=	electric field due to the applied voltage ($V\ cm^{-1}$)
$\mathbf{E}_\rho$	=	electric field due to space charge ($V\ cm^{-1}$)
d	=	domain length (cm)
k_B	=	Boltzmann constant ($erg\ K^{-1}$)
T_e	=	electron temperature (K)
T_g	=	gas temperature (K)
$m_{e,k}$	=	electron/ion mass (g)

*Graduate Research Assistant, Department of Aerospace Engineering, The University of Texas at Austin.
†Graduate Research Assistant, Department of Aerospace Engineering, The University of Texas at Austin.
‡Professor, Department of Aerospace Engineering, The University of Texas at Austin.

V_k = ion drift velocity (cm s^{-1})

II. Introduction

Gaseous mediums, when exposed to sufficiently strong electric fields, can become rapidly ionized through an electron avalanche, which leads to breakdown of the gas. This breakdown is characterized by sharp space charge gradients ahead of the electron avalanche, which can induce electric fields that are themselves strong enough to produce rapid ionization ahead of the avalanche. This results in the formation of a self-propagating streamer [1–3], which is governed by highly nonlinear and tightly coupled physical processes.

Streamers have have found use in a wide range of practical applications, in areas such as combustion [4–7], aerodynamic flow actuation [8, 9], biological decontamination through generation of reactive species [10, 11], and hydrocarbon reforming [12, 13]. Simulations of streamers within these applications, however, has proven to be a significant challenge. The time scales typically associated with the evolution of streamers, for instance the advective, dielectric, and effective ionization time scales [14] (which typically fall within the sub-nanosecond to sub-picosecond range), are often considerably smaller than the time scales driven by the application of interest (for instance, flow actuation and combustion can evolve on second and millisecond scales). Additionally, the length scales that typically define the plasma, for instance the Debye length, can be on the order of microns or smaller under atmospheric conditions [15]. As such, the application of ideally suited numerical methods is of central importance.

Typically, streamers are modeled as a plasma fluid, with a set of transport equations for the electron and ions, which are governed by the drift-diffusion approximation. This is coupled with Poisson's equation for the electric potential, which relates space charge and the electric field. Bulk fluid transport is often neglected, as the time scales over which streamers evolve (O(1-100 ns), given streamer propagation speeds of 10^7-10^8 cm s^{-1} [16] in gaps sizes typically on the order of centimeters) are several orders of magnitudes smaller than the time scales of fluid movement.

A range of kinetic models can be used to describe the streamer dynamics. More nuanced models that include several ions, and reactions describing ionization, dissociative and ion-ion recombination, electron attachment and detachment, and other processes are often used in one and two-dimensional models [17]. Three-dimensional simulations typically rely on using simplified kinetics mechanisms, given the high computation costs [18].

In order to address the difficulties described above, a variety of numerical techniques have been explored. Earlier approaches [19, 20] generally relied on an explicit treatment of the transport equations. In order to ease time step restrictions, more recent approaches have involved semi-implicit [21, 22] and fully implicit approaches [23, 24] (although most fully implicit approaches still rely on an explicit prediction of the source terms for evaluation of the Poisson equation).

In this work, a semi-implicit spectral deferred correction (SDC) type approach is explored through a series of dark discharge simulations in one dimension. In section III, the plasma model (including the governing equations, numerical approach, kinetics model, boundary conditions, and initial conditions) are discussed. Results from the SDC simulations are compared against solutions from a boundary value problem (BVP) solver, and physical characteristics are discussed in section IV. In section V, insights drawn from the previous section are used to gain insight into the resolution and time step size requirements, and conclusion are presented in section VI.

III. Numerical Model

A hydrodynamic model for solving streamer discharges in air at atmospheric pressure and 300 K is employed. In order to simplify the equations, it is assumed that the transport of neutral species due to bulk velocity and diffusion is negligible due to the short time scales typically associated with streamer propagation ($O(1-100)$ ns). The adoption of a drift-diffusion model for the electron and ion fluxes results in a set of transport equations for the electron and ions

$$\frac{\partial n_e}{\partial t} = \nabla \cdot (n_e \mu_e \mathbf{E}) + \nabla \cdot (\mathcal{D}_e \nabla n_e) + \dot{\omega}_e \tag{1}$$

$$\frac{\partial n_k}{\partial t} = -\nabla \cdot (Z_k n_k \mu_k \mathbf{E}) + \nabla \cdot (\mathcal{D}_k \nabla n_k) + \dot{\omega}_e, \tag{2}$$

along with Gauss's law

$$\varepsilon_0 \varepsilon_r \nabla^2 \phi = e \left(\sum_{k=1}^{N_i} Z_k n_k \right) - e n_e. \tag{3}$$

In equations 1 and 2, the first and second terms on the right hand side represent the advective and diffusive source terms, $\mathbf{A}_{e,k}$ and $\mathbf{D}_{e,k}$, respectively. A local field approximation is used to model the electron and ion transport coefficients, as well as the rate coefficients of select reactions, as functions of the reduced electric field E/N.

These equations are solved with a finite volume approximation in a one-dimensional domain of length d, with values located at the cell-centers. The domain represents the gap between two electrodes, with the anode located at the left side of the domain ($x = 0$) and the cathode located at the right ($x = d$). In order to adequately resolve the thin diffusive layers near the electrodes, a constant stretch rate α ($\Delta x_{i+1} = \Delta_i \alpha$) is used to generate a grid (in this study, $1.01 < \alpha < 1.1$). The grid is symmetric across the center of the domain.

A. Time Advancement Algorithms

A MISDC strategy [25, 26] is used for time advancement of the system. The advantage of this approach is that it provides a solution of arbitrary order in time through iterative approximations to the previous solution. In order to advance the system from time $t = n$ to $t = n + 1$, $k = 1, k_{\max}$ iterations are performed, where $k_{\max}$ controls the order of accuracy in time. A minimum of two iterations are required to achieve second-order accuracy in time.

Each time step begins by using the solution from the previous time step as the initial solution vector at the next time $\mathbf{U}^{n+1,k=0} = \mathbf{U}^n$ and $\phi^{n+1,k=0} = \phi^n$, where the state vector $\mathbf{U}$ consists of the electron and ion number densities. Each iteration begins with calculation of the thermochemical properties based on the data from the previous iteration ($\mathbf{U}^{n+1,k}$). Next, provisional time-advanced state variables are calculated implicitly via

$$\frac{\mathbf{U}_{AD}^{k+1} - \mathbf{U}^n}{\Delta t} = \underbrace{\mathbf{A}_{\mathbf{U}}^{n+1/2,k} + (\mathbf{D}_{\mathbf{U}})_{AD}^{k+1} + \frac{1}{2}(\mathbf{D}_{\mathbf{U}}^k - \mathbf{D}_{\mathbf{U}}^n)}_{Q_{\mathbf{U}}^{k+1}} + I_{R,\mathbf{U}}^k. \tag{4}$$

In the above formulation, $\mathbf{D}_{\mathbf{U}}^k$ and $\mathbf{D}_{\mathbf{U}}^n$ are evaluated explicitly using data from the previous iteration and previous time step, respectively, while the advective operator is obtained explicitly using time-centered edge states from a second-order Godunov method [27]. Reactions are accounted for using the time-lagged reactive term $I_{R,\mathbf{U}}^k$.

Next, the state is updated via

$$\frac{\partial \mathbf{U}}{\partial t} = \dot{\omega}(\mathbf{U}) + Q_{\mathbf{U}}^{k+1}, \tag{5}$$

using the implicit, variable-order BDF method available in CVODE [28] to integrate the reactive source term from $t = n$ to $t = n + 1$. Solution of this system yields the state variables at the next iteration $\mathbf{U}^{n+1,k+1}$, which can be used to update the time-lagged reactive source term

$$I_{\mathbf{U}}^{k+1} = \frac{\mathbf{U}^{k+1} - \mathbf{U}^k}{\Delta t} - Q_{\mathbf{U}}^{k+1}. \tag{6}$$

Finally, the updated state variables are used to calculate the potential ϕ^{k+1}.

B. Electric Field Calculations

The electric field used to calculate the drift velocities and evaluate select thermochemical quantities is written as the sum of two components $\mathbf{E} = \mathbf{E}_0 + \mathbf{E}_\rho$. The first components represents the electric field due to the voltage applied across the electrodes, assumed uniform in space in the present configuration. The second component represents the electric field due to space charge, which obeys a boundary value problem consisting of equation 3 with zero Dirichlet boundary conditions.

In order to account for multidimensional space charge effects, an approximation of the Poisson equation is used for calculation of the electric field [29, 30], in which it assumed that the charge density at each point in the domain is distributed uniformly across a disk of prescribed radius r. Calculation of the space charge-induced electric field then becomes

$$\mathbf{E}_\rho(x) = \int_{-x}^{d-x} -\frac{\rho(x + x')}{2\varepsilon_0 \varepsilon_r} \left(\frac{x'}{\sqrt{r^2 + x'^2}} + \mathrm{sgn}(x')1 \right) dx'. \tag{7}$$

In order to account for the boundary conditions, image charges extending a length d from the left and right boundary of the domain are included. As expected, letting $r \to \infty$ results in a solution that matches that obtained by solving the Poisson equation in a one-dimensional cartesian domain (3).

C. Chemical Kinetics Mechanism

The kinetics mechanism used to describe air plasma chemistry is adapted from [20]. The mechanism describes the generation of electrons through direct electron impact ionization, electron attachment, various ion-neutral interactions, dissociative recombination, and ion-ion recombination. Electron attachment rates in [17] are used instead of those in [20]. Electron detachment is also considered for both low [31] and high [32] electric field strengths. Finally, a volumetric ionization source term is included, accounting for charge generation due to radioactive decay (e.g. due to radon in air) and cosmic rays. The full set of species includes the electron (E), positive and negative ions (O_2^+, N_2^+, O_4^+, N_4^+, $O_2^+N_2$, and O_2^-), and neutral species (O_2, N_2, and O).

The full set of reactions used in the model includes electron impact reactions

$$\mathrm{E} + \mathrm{N_2} \rightarrow \mathrm{E} + \mathrm{E} + \mathrm{N_2^+} \tag{R1}$$
$$\mathrm{E} + \mathrm{O_2} \rightarrow \mathrm{E} + \mathrm{E} + \mathrm{O_2^+}, \tag{R2}$$

conversion of N_2^+ to O_2^+

$$\mathrm{N_2^+} + \mathrm{N_2} + \mathrm{M} \rightarrow \mathrm{N_4^+} + \mathrm{M} \tag{R3}$$
$$\mathrm{N_4^+} + \mathrm{O_2} \rightarrow \mathrm{O_2^+} + \mathrm{N_2} + \mathrm{N_2} \tag{R4}$$
$$\mathrm{N_2^+} + \mathrm{O_2} \rightarrow \mathrm{O_2^+} + \mathrm{N_2}, \tag{R5}$$

conversion of O_2^+ to O_4^+

$$\mathrm{O_2^+} + \mathrm{N_2} + \mathrm{N_2} \rightarrow \mathrm{O_2^+N_2} + \mathrm{N_2} \tag{R6}$$
$$\mathrm{O_2^+N_2} + \mathrm{N_2} \rightarrow \mathrm{O_2^+} + \mathrm{N_2} + \mathrm{N_2} \tag{R7}$$
$$\mathrm{O_2^+N_2} + \mathrm{O_2} \rightarrow \mathrm{O_4^+} + \mathrm{N_2} \tag{R8}$$
$$\mathrm{O_2^+} + \mathrm{O_2} + \mathrm{M} \rightarrow \mathrm{O_4^+} + \mathrm{M}, \tag{R9}$$

dissociative and ion-ion recombination

$$\mathrm{E} + \mathrm{O_4^+} \rightarrow \mathrm{O_2} + \mathrm{O_2} \tag{R10}$$
$$\mathrm{E} + \mathrm{O_2^+} \rightarrow \mathrm{O} + \mathrm{O} \tag{R11}$$
$$\mathrm{O_2^-} + \mathrm{O_4^+} \rightarrow \mathrm{O_2} + \mathrm{O_2} + \mathrm{O_2} \tag{R12}$$
$$\mathrm{O_2^-} + \mathrm{O_4^+} + \mathrm{M} \rightarrow \mathrm{O_2} + \mathrm{O_2} + \mathrm{O_2} + \mathrm{M} \tag{R13}$$
$$\mathrm{O_2^-} + \mathrm{O_2^+} + \mathrm{M} \rightarrow \mathrm{O_2} + \mathrm{O_2} + \mathrm{M}, \tag{R14}$$

electron attachment and detachment

$$\mathrm{E} + \mathrm{O_2} + \mathrm{O_2} \rightarrow \mathrm{O_2^-} + \mathrm{O_2} \tag{R15}$$
$$\mathrm{E} + \mathrm{O_2} + \mathrm{N_2} \rightarrow \mathrm{O_2^-} + \mathrm{N_2} \tag{R16}$$
$$\mathrm{O_2^-} + \mathrm{O_2} \rightarrow E + 2\mathrm{O_2} \tag{R17}$$
$$\mathrm{O_2^-} + \mathrm{N_2} \rightarrow E + \mathrm{O_2} + \mathrm{N_2} \tag{R18}$$

and generation of electrons via volumetric sources (primarily radioactive decay of radon-222, see section III.E for further detail)

$$\mathrm{O_2} \rightarrow E + \mathrm{O_2^+} \tag{R19}$$
$$\mathrm{N_2} \rightarrow E + \mathrm{N_2^+}. \tag{R20}$$

Since the rate coefficients for dissociative recombination and electron detachment are functions of the electron temperature T_e, data from BOLSIG+ [33] are used to fit the electron temperature as a function of the reduced electric field strength ($T_e = f(E/N)$).

It is is found that most of the ions are produced and consumed on very short time scales. Thus, a quasi-steady state assumption is adopted, whereby O_2^+, N_2^+, N_4^+, and $O_2^+N_2$ are assumed to be in equilibrium. Under this assumption, only the electron, one positive ion (O_4^+), and one negative ion (O_2^-) are transported, thus reducing computational costs.

D. Boundary Conditions

Boundary conditions for the electric potential are Dirichlet conditions, with a non-zero value applied at one of the boundaries (the driven electrode), and a value of zero at the other boundary (the grounded electrode).

Following the approach in [34], the species number density boundary conditions are affected by the relative magnitudes of the thermal and drift velocities. For the electron, it is found that for the conditions of interest, the thermal velocity

$$\bar{v}_e = \sqrt{\frac{8k_B T_e}{\pi m_e}} \tag{8}$$

dominates over the drift velocity, and the flux directed into the left and right boundaries is

$$\Gamma_{e,x} = \frac{1}{2} n_e \bar{v}_e. \tag{9}$$

Note that the flux used in this study is greater than that used in similar studies by a factor of 2. This flux can be modified to take into account the emission of electrons from the cathode as

$$\Gamma_{e,c} = \frac{1}{2} n_e \bar{v}_e - 2\Gamma_{em}. \tag{10}$$

The emission of electrons can be due to the collision of ions with the cathode, in which case Γ_{em} can be given as

$$\Gamma_{em} = \gamma \sum_k \Gamma_{k,c}, \tag{11}$$

where $\Gamma_{k,c}$ is the flux of ion k at the cathode boundary, and γ is the secondary electron emission coefficient (taken to be 0.05 [35]). Alternatively, a constant electron emission at the cathode n_{em} at the cathode can be specified, resulting in

$$\Gamma_{e,c} = \frac{1}{2} \bar{v}_e (n_e - n_{em}). \tag{12}$$

Note that it is assumed that the electrode is an absolutely absorbing surface (meaning none of the particles that impact the electrode surface are reflected).

Calculation of the boundary conditions for positive and negative ions is more complex, as the relative importance of the drift and thermal velocities changes depending on the strength of the applied electric field. Under the *weak-field* assumption [34], the drift velocity is negligible and the boundary-directed fluxes are calculated in the same manner as for the electron,

$$\Gamma_{k,x} = \frac{1}{2} n_k \bar{v}_k, \tag{13}$$

where the ion thermal velocity is calculated using the gas temperature T_g, and the ion mass m_k.

Under the *strong-field* assumption, the ion drift velocity dominates over the thermal velocity. For positive ions, the boundary conditions at the cathode become

$$\Gamma_{k,x} = n_k V_k \quad (\text{for } E_x > 0) \tag{14}$$

$$\Gamma_{k,x} \approx 0 \quad (\text{for } E_x < 0), \tag{15}$$

with the drift velocity calculated as $V_k = Z_k \mu_k E_x$. At the anode, the opposite conditions hold true

$$\Gamma_{k,x} = n_k V_k \quad (\text{for } E_x < 0) \tag{16}$$

$$\Gamma_{k,x} \approx 0 \quad (\text{for } E_x > 0). \tag{17}$$

These strong-field conditions can be succinctly summarized by concluding that the ion flux at a given electrode boundary is $n_k V_k$ if the ion velocity is directed from the plasma towards the wall, and zero otherwise. Similar boundary conditions for the negative ions are constructed using the same approach.

E. Initial Conditions

It has been found in previous studies ([36, 37]) that initial conditions can impact streamer characteristics, especially in the early stages of propagation. In order to construct initial conditions that adequately capture physical processes, we start by considering the radioactive decay of gaseous nuclides, specifically radon-222 (^{222}Rd), which is present in air in trace amounts. When it decays, ^{222}Rd is known to emit alpha particles with high energies (4.99 or 5.49 MeV), capable of ionizing neutral species.

Due to the isotropic nature of the alpha particle emission, this is treated as a volumetric source of ionization, occurring at the same rate everywhere in the domain. Following the work in [38], this source term is approximately $S = 10^1$ cm^{-3} s^{-1} under atmospheric conditions, and contributes to the production of electrons, as well as N_2^+ and O_2^+. In order to construct initial conditions, a simulation with no initial charged particles or electric field is run, until a steady state is reached (occurring once the volumetric source term reaches an equilibrium with the diffusive losses at the electrode boundaries). Given the absence of an applied electric field, the weak-field boundary assumptions are used to evaluate the ion fluxes. This steady state is used as the initial condition for all subsequent simulations.

The steady state solution is composed primarily of O_4^+ and O_2^- ions, as the electric field is low enough to allow for high rates of electron attachment. This differs from approaches typically used in streamer simulations, where an initial distribution of seed electrons and positive ions is often assumed. The initial electron and ion profiles are provided in Fig. 1.

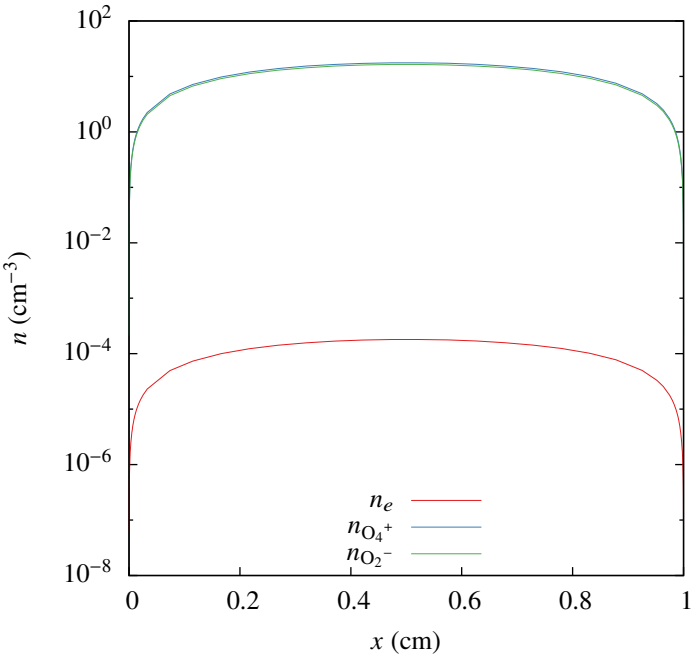

Fig. 1 Initial conditions for the electrons and ions.

IV. Streamer Simulations

The accuracy and robustness of the SDC method is evaluated by considering a suite of test cases. The test cases are comprised of various steady state solutions, so-called dark discharges, which are obtained under an applied electric field E_0 that is uniform in space and time. The applied electric field must be sufficiently strong to produce a non-negligible degree of ionization, but weak enough to prevent the formation of an unsteady self-propagating streamer. In order to assess the accuracy of the method, solutions obtained using the SDC approach are compared against solutions for the same problem from the boundary value problem solver bvp4c available in MATLAB.

Each test case features a constant applied reduced electric field of 100 Td directed in the positive x-direction in a domain of air under atmospheric conditions. The transport equations are solved on a one-dimensional stretched grid, with the chemistry and initial conditions as described in section III. The grid features cells adjacent to the electrons have

a grid spacing of $\Delta x_{\min} = 10^{-4}$ cm, a stretching rate of $\alpha = 1.018$, and a total of 500 points. A constant time step size of $\Delta t = 10$ ps is required to satisfy the CFL condition

$$\sigma = \frac{E_0 \mu_e \Delta t}{\Delta x_{\min}}, \quad 0 \leq \sigma \leq 1 \tag{18}$$

due to the explicit electron advection and the micron grid spacing near the electrodes. Note that although also handled explicitly, ion drift does not need to be considered when evaluating the CFL condition, as their relatively large mass results in a much smaller drift velocity.

Transport coefficients for the electron are taken to be constant, and are evaluated at a reduced electric field strength of 100 Td using BOLSIG+ [33] and cross section data from the LXCat database [39]. Ions mobilities and diffusivities are evaluated using cross section data as described in [40]. A disk radius of $r \to \infty$ is used, yielding a solution equal to that obtained by solving a one dimensional Poisson problem for the potential. Simulations are run until a steady solution is reached.

In order to understand how different physical processes govern the dark discharge, the electron flux at the cathode $\Gamma_{e,c}$ is modified to elicit different behaviors. In test cases A1 and A2, the electron emission flux Γ_{em} is determined based on the flux of ions to the cathode, as described in equation 11. In test case A1, space charge effects on the electric field are considered, while they are neglected in case A2 ($E_\rho = 0$). Comparisons between the SDC approach and the BVP solver for test case A1 are presented in Fig. 2.

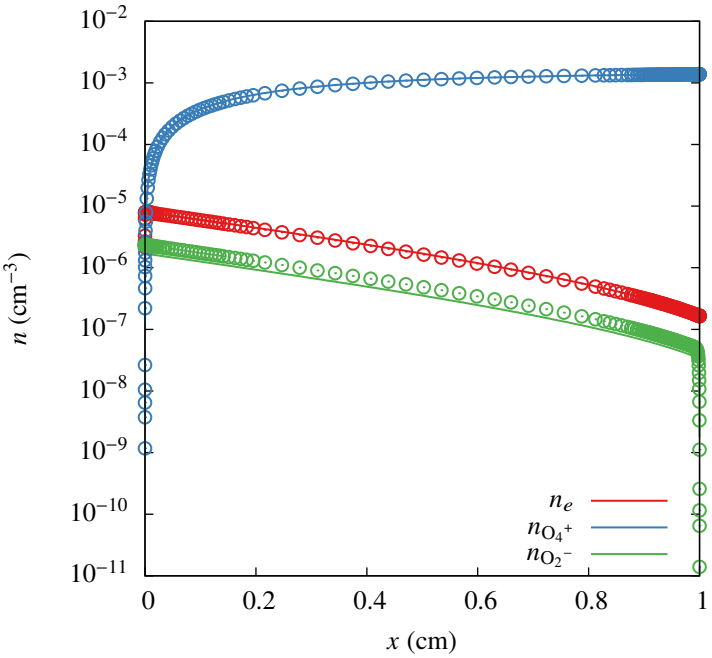

Fig. 2 Steady state number density profiles for the electron, positive ion, and negative ion in the A1 case. Results from the SDC approach (solid lines) are compared against the results from the BVP solver (circular markers).

Several trends and features are apparent. First, the positive and negative ions display maximum values at the cathode and anode respectively, following the drift induced by the electric field. The electrons also reach a maximum value near the anode, but support a sharp diffusive layer in that region as well (as do the positive and negative ions near the anode and cathode, respectively). Throughout most of the channel, the profiles are dominated by a balance between drift and reactive processes. Near the electrodes, however, diffusion also begins to play an important role, and the profiles are characterized by a balance between all three processes. The impact of the space charge-induced electric field can be considered by examining the solutions for the A2 test case in Fig. 3, which do not take into account the space charge-induced electric field.

Evidently, the profiles do not change noticeably, indicating that the electric field is dominated by the applied component ($|\mathbf{E}_0| \gg |\mathbf{E}_\rho|$). This can be seen clearly in Fig. 4, which shows the reduced electric field components and

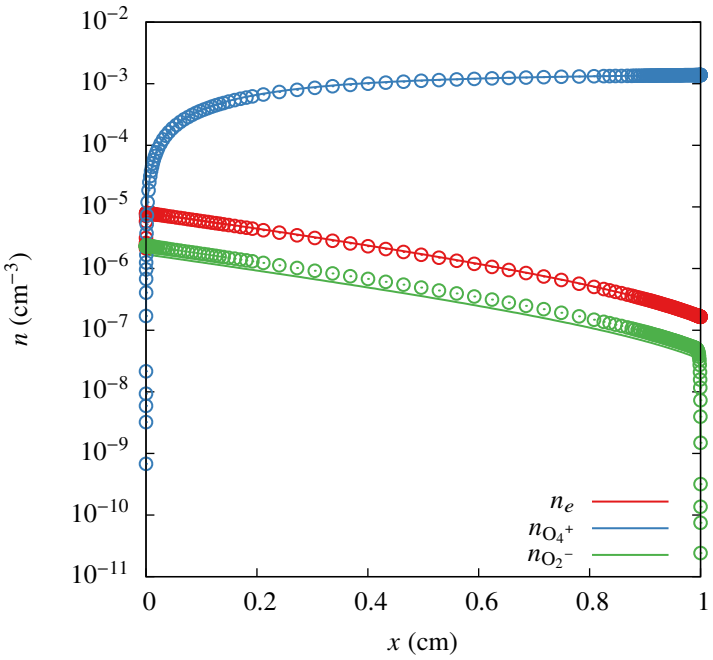

Fig. 3 Steady state number density profiles for the electron, positive ion, and negative ion in the A2 case. Results from the SDC approach (solid lines) are compared against the results from the BVP solver (circular markers).

charge density. It is evident that although there is a small positive space charge across the gap, its contribution to the

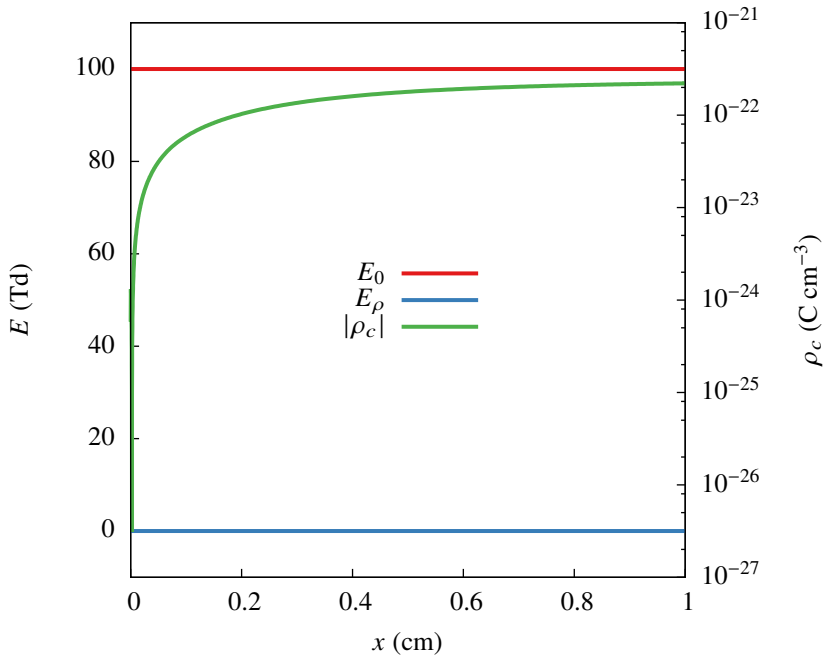

Fig. 4 Steady state reduced electric field components and space charge density through the gap in the A1 case.

electric field is negligible.

In order to examine a steady state configuration where E_ρ has an appreciable impact on the results, we consider the

B1 and B2 test cases. In these test cases, electron emissions from the cathode are instead given by equation 12, with a constant value of $n_{em} = 10 \times 10^7$ cm^{-3}. The electron emissions at the cathode are significant enough to create a space charge in the domain that induces an electric field E_ρ that is of the same order as the applied electric field. In the B1 test case, the impact of space charge effects on the electric field are taken into account, while they are neglected in the B2 test case. Results for the B1 and B2 test cases are presented in Fig. 5 and Fig. 6.

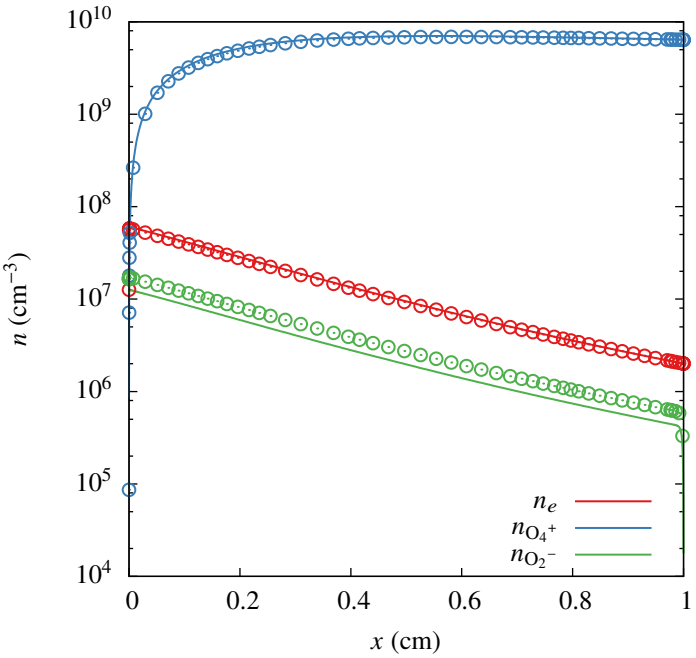

Fig. 5 Steady state number density profiles for the electron, positive ion, and negative ion in the B1 case. Results from the SDC approach (solid lines) are compared against the results from the BVP solver (circular markers).

It is clear that E_ρ plays a more significant role in the second set of test cases (for instance, inclusion of space charge effects results in an electron number density peak that is 34% lower than when it is neglected). Further insight can be gained by looking at profiles of the steady state electric field components, and space charge in the domain.

As before, there is an abundance of positive space charge throughout the gap. This can be attributed to a high electron temperature ($T_e \approx 2 \times 10^4$ K at 100 Td) which induces a much larger electron flux at the electrodes as compared with positive ions. Although not visible on the plot, there is a small region of negative space charge near the anode. This produces the space charge-induced electric field profile E_ρ with negative values near the anode and positive values near the cathode.

V. Grid and Time Step Requirements

Diffusive electron losses at the anode create a sheath region with sharp gradients that present significant numerical challenges. High spatial resolution is required in this region in order to resolve the electron and ion profiles accurately, which is crucial for evaluating the fluxes at the boundary. Additional simulations of the A1 test case are performed with varying resolution near the electrodes. In case A1R1, the minimum grid spacing is reduced by an order of magnitude ($\Delta x_{\text{min}} = 10^{-5}$ cm), while retaining 500 points ($\alpha = 1.0296$). For the second refined case (A1R2), 500 points are again used, with $\Delta x_{\text{min}} = 10^{-6}$ cm and $\alpha = 1.04$. The electron profiles near the anode for the three cases are compared in Fig. 8.

It is apparent that if one wants to accurately capture the electron profile at the boundary, grid spacing significantly finer than those typically used in streamer simulations (by an order or two of magnitude) is required. This has severe numerical implications, as the explicit electron advection necessitates a reduction in the time step size by the same factor. The A1R1 test case requires a time step size $\Delta t = 1$ ps, while A1R2 requires $\Delta t = 0.1$ ps.

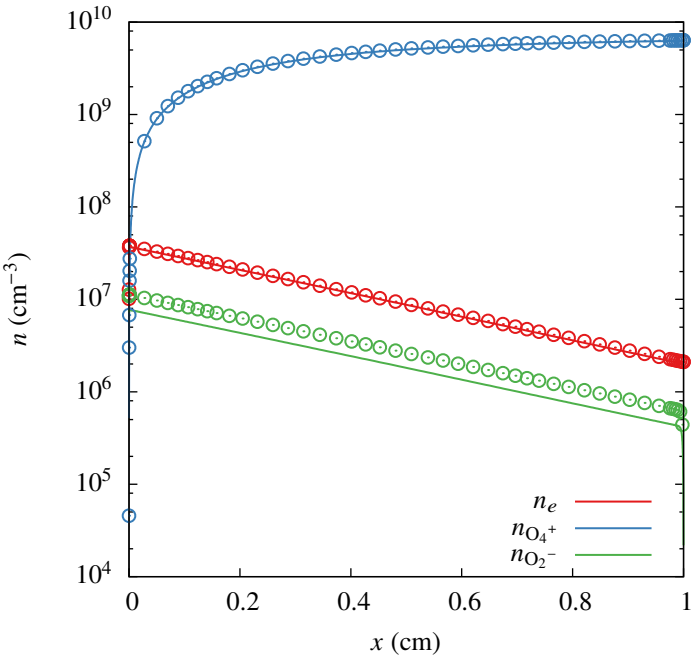

Fig. 6 Steady state number density profiles for the electron, positive ion, and negative ion in the B2 case. Results from the SDC approach (solid lines) are compared against the results from the BVP solver (circular markers).

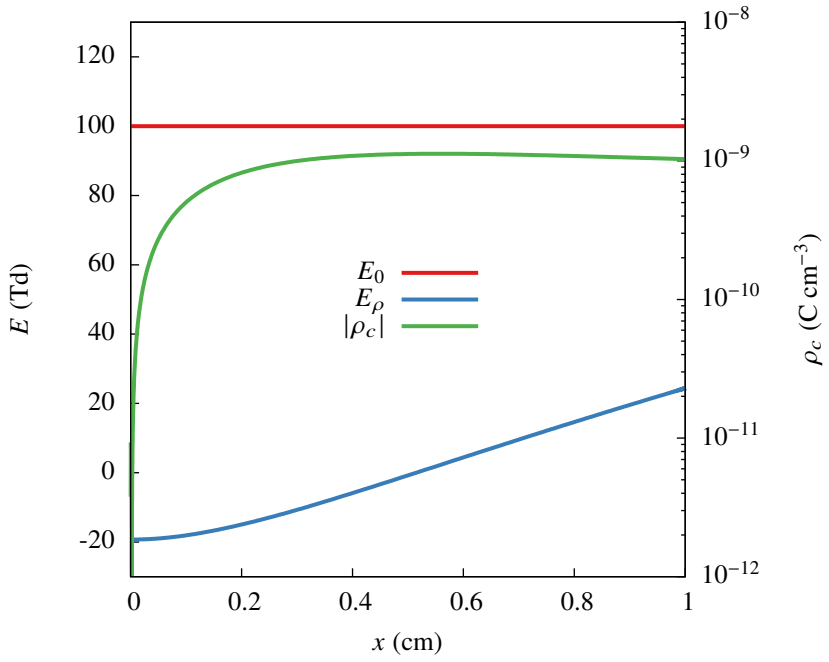

Fig. 7 Steady state reduced electric field components and space charge density through the gap in the B1 case.

It is not uncommon to use a sub-picosecond time step size in the simulation of unsteady propagating streamers. However, when one considers that the reduced electric fields in such cases is greater by a factor of five or more, the corresponding increase in the electron drift velocity implies $\Delta t = 0.01$ ps, or smaller. It is apparent that improvements

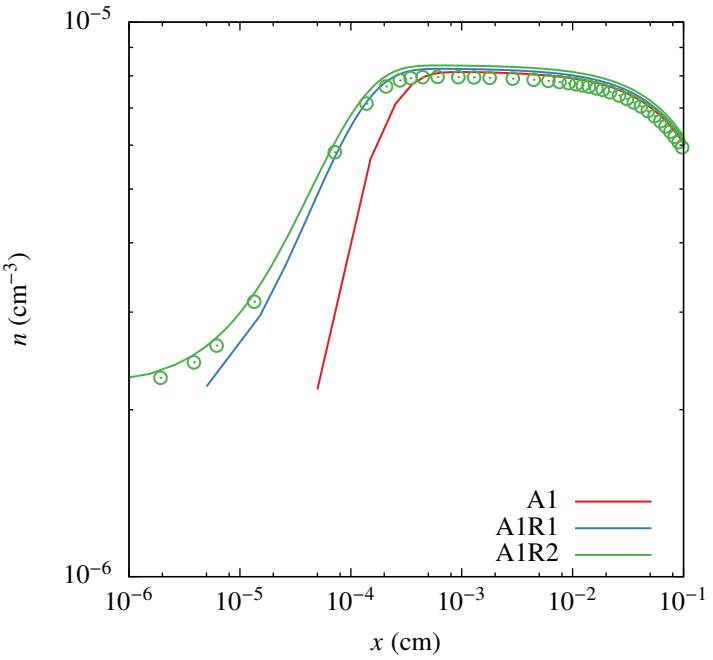

Fig. 8 Electron profile in the region near the anode for the A1 test case with various resolutions.

to the approach are needed in order to conduct simulations of practical interest.

VI. Conclusion

Simulations of various dark discharge solutions were performed using a MISDC approach to advance a plasma model consisting of equations for the electron, positive and negative ions, and a Poisson equation for the potential to a steady state solution. Accurate boundary conditions were applied under the assumption of a strong electric field near the electrodes, and initial conditions were constructed by considering the balance of charge generation through the radioactive decay of ^{222}Rd, and diffusive losses at the electrodes. A chemical kinetics model for air-plasma chemistry consisting of reactions describing electron impact ionization, electron attachment, various ion-neutral interactions, dissociative recombination, and ion-ion recombination was used, and simplifications were made by assuming certain ions exist in a quasi-steady state.

Results were compared against solutions from the BVP solver in MATLAB to ensure accuracy, and insights into physical characteristics of the problem were drawn. It was observed that sharp gradients near the electrodes necessitated grid spacing on the order of 10^{-6} microns to accurately resolve the solution, along with time steps sizes on the order of 0.01 ps. This implies even more severe restrictions for unsteady propagating streamers, highlighting the need for improvements to the numerical methods used to solve such problems. Improvements to the methods aimed at circumventing the restrictions imposed by the electron advective and dielectric time scales will be the focus of future work.

Acknowledgments

Nicholas Deak and Fabrizio Bisetti are supported in part by NSF grant 1903775.

References

[1] Bogaerts, A., Neyts, E., Gijbels, R., and Van der Mullen, J., "Gas discharge plasmas and their applications," *Spectrochimica Acta Part B: Atomic Spectroscopy*, Vol. 57, No. 4, 2002, pp. 609–658.

[2] Ebert, U., Montijn, C., Briels, T. M., Hundsdorfer, W., Meulenbroek, B., Rocco, A., and van Veldhuizen, E. M., "The multiscale nature of streamers," *Plasma Sources Science and Technology*, Vol. 15, No. 2, 2006, p. S118.

[3] Pancheshnyi, S., Nudnova, M., and Starikovskii, A., "Development of a cathode-directed streamer discharge in air at different pressures: experiment and comparison with direct numerical simulation," *Physical Review E*, Vol. 71, No. 1, 2005, p. 016407.

[4] Ju, Y., and Sun, W., "Plasma assisted combustion: Dynamics and chemistry," *Progress in Energy and Combustion Science*, Vol. 48, 2015, pp. 21–83.

[5] Starikovskiy, A., and Aleksandrov, N., "Plasma-assisted ignition and combustion," *Progress in Energy and Combustion Science*, Vol. 39, No. 1, 2013, pp. 61–110.

[6] Sharma, A., Subramaniam, V., Solmaz, E., and Raja, L. L., "Fully coupled modeling of nanosecond pulsed plasma assisted combustion ignition," *Journal of Physics D: Applied Physics*, Vol. 52, No. 9, 2018, p. 095204.

[7] Deak, N., Bellemans, A., and Bisetti, F., "Plasma-assisted ignition of methane/air and ethylene/air mixtures: Efficiency at low and high pressures," *Proceedings of the Combustion Institute*, 2020.

[8] Moreau, E., "Airflow control by non-thermal plasma actuators," *Journal of physics D: applied physics*, Vol. 40, No. 3, 2007, p. 605.

[9] Starikovskii, A. Y., Nikipelov, A., Nudnova, M., and Roupassov, D., "SDBD plasma actuator with nanosecond pulse-periodic discharge," *Plasma Sources Science and Technology*, Vol. 18, No. 3, 2009, p. 034015.

[10] Akiyama, H., "Streamer discharges in liquids and their applications," *IEEE Transactions on dielectrics and electrical Insulation*, Vol. 7, No. 5, 2000, pp. 646–653.

[11] Lukes, P., Appleton, A. T., and Locke, B. R., "Hydrogen peroxide and ozone formation in hybrid gas-liquid electrical discharge reactors," *IEEE Transactions on Industry Applications*, Vol. 40, No. 1, 2004, pp. 60–67.

[12] Lukes, P., and Locke, B. R., "Plasmachemical oxidation processes in a hybrid gas–liquid electrical discharge reactor," *Journal of Physics D: Applied Physics*, Vol. 38, No. 22, 2005, p. 4074.

[13] Levko, D., Sharma, A., and Raja, L. L., "Plasmas generated in bubbles immersed in liquids: direct current streamers versus microwave plasma," *Journal of Physics D: Applied Physics*, Vol. 49, No. 28, 2016, p. 285205.

[14] Vitello, P., Penetrante, B., and Bardsley, J., "Simulation of negative-streamer dynamics in nitrogen," *Physical Review E*, Vol. 49, No. 6, 1994, p. 5574.

[15] Unfer, T., Boeuf, J.-P., Rogier, F., and Thivet, F., "An asynchronous scheme with local time stepping for multi-scale transport problems: Application to gas discharges," *Journal of Computational Physics*, Vol. 227, No. 2, 2007, pp. 898–918.

[16] Kulikovsky, A., "Positive streamer in a weak field in air: A moving avalanche-to-streamer transition," *Physical Review E*, Vol. 57, No. 6, 1998, p. 7066.

[17] Kossyi, I., Kostinsky, A. Y., Matveyev, A., and Silakov, V., "Kinetic scheme of the non-equilibrium discharge in nitrogen-oxygen mixtures," *Plasma Sources Science and Technology*, Vol. 1, No. 3, 1992, p. 207.

[18] Pancheshnyi, S., Ségur, P., Capeillère, J., and Bourdon, A., "Numerical simulation of filamentary discharges with parallel adaptive mesh refinement," *Journal of Computational Physics*, Vol. 227, No. 13, 2008, pp. 6574–6590.

[19] Kulikovsky, A., "Two-dimensional simulation of the positive streamer in N2 between parallel-plate electrodes," *Journal of Physics D: Applied Physics*, Vol. 28, No. 12, 1995, p. 2483.

[20] Pancheshnyi, S., and Starikovskii, A. Y., "Two-dimensional numerical modelling of the cathode-directed streamer development in a long gap at high voltage," *Journal of Physics D: Applied Physics*, Vol. 36, No. 21, 2003, p. 2683.

[21] Teunissen, J., and Ebert, U., "Afivo: A framework for quadtree/octree AMR with shared-memory parallelization and geometric multigrid methods," *Computer Physics Communications*, Vol. 233, 2018, pp. 156–166.

[22] Marskar, R., "An adaptive Cartesian embedded boundary approach for fluid simulations of two-and three-dimensional low temperature plasma filaments in complex geometries," *Journal of Computational Physics*, Vol. 388, 2019, pp. 624–654.

[23] Van Dijk, J., Peerenboom, K., Jimenez, M., Mihailova, D., and Van der Mullen, J., "The plasma modelling toolkit Plasimo," *Journal of Physics D: Applied Physics*, Vol. 42, No. 19, 2009, p. 194012.

[24] Breden, D., Raja, L. L., Idicheria, C. A., Najt, P. M., and Mahadevan, S., "A numerical study of high-pressure non-equilibrium streamers for combustion ignition application," *Journal of Applied Physics*, Vol. 114, No. 8, 2013, p. 083302.

[25] Esclapez, L., Ricchiuti, V., Bell, J. B., and Day, M. S., "A spectral deferred correction strategy for low Mach number reacting flows subject to electric fields," *Combustion Theory and Modelling*, Vol. 24, No. 2, 2020, pp. 194–220.

[26] Nonaka, A., Bell, J., Day, M., Gilet, C., Almgren, A., and Minion, M., "A deferred correction coupling strategy for low Mach number flow with complex chemistry," *Combustion Theory and Modelling*, Vol. 16, No. 6, 2012, pp. 1053–1088.

[27] Almgren, A. S., Bell, J. B., Colella, P., Howell, L. H., and Welcome, M. L., "A conservative adaptive projection method for the variable density incompressible Navier–Stokes equations," *Journal of computational Physics*, Vol. 142, No. 1, 1998, pp. 1–46.

[28] Hindmarsh, A. C., Brown, P. N., Grant, K. E., Lee, S. L., Serban, R., Shumaker, D. E., and Woodward, C. S., "SUNDIALS: Suite of nonlinear and differential/algebraic equation solvers," *ACM Transactions on Mathematical Software (TOMS)*, Vol. 31, No. 3, 2005, pp. 363–396.

[29] Davies, A., Evans, C., and Jones, F. L., "Electrical breakdown of gases: the spatio-temporal growth of ionization in fields distorted by space charge," *Proceedings of the Royal Society of London. Series A. Mathematical and Physical Sciences*, Vol. 281, No. 1385, 1964, pp. 164–183.

[30] Pumplin, J., "Application of Sommerfeld-Watson transformation to an electrostatics problem," *American Journal of Physics*, Vol. 37, No. 7, 1969, pp. 737–739.

[31] Aleksandrov, N., and Anokhin, E., "Low-energy electron attachment and detachment in vibrationally excited oxygen," *Journal of Physics D: Applied Physics*, Vol. 42, No. 22, 2009, p. 225210.

[32] Ponomarev, A., and Aleksandrov, N., "Monte Carlo simulation of electron detachment properties for ions in oxygen and oxygen: nitrogen mixtures," *Plasma Sources Science and Technology*, Vol. 24, No. 3, 2015, p. 035001.

[33] Hagelaar, G., and Pitchford, L., "Solving the Boltzmann equation to obtain electron transport coefficients and rate coefficients for fluid models," Vol. 14, No. 4, 2005, p. 722.

[34] Gorin, V., Kudryavtsev, A., Yao, J., Yuan, C., and Zhou, Z., "Boundary conditions for drift-diffusion equations in gas-discharge plasmas," *Physics of Plasmas*, Vol. 27, No. 1, 2020, p. 013505.

[35] Nagaraja, S., Yang, V., and Adamovich, I., "Multi-scale modelling of pulsed nanosecond dielectric barrier plasma discharges in plane-to-plane geometry," *Journal of Physics D: Applied Physics*, Vol. 46, No. 15, 2013, p. 155205.

[36] Nijdam, S., Wormeester, G., Van Veldhuizen, E., and Ebert, U., "Probing background ionization: positive streamers with varying pulse repetition rate and with a radioactive admixture," *Journal of Physics D: Applied Physics*, Vol. 44, No. 45, 2011, p. 455201.

[37] Zhu, Y., Zhang, X., and He, J., "Predicting streamer discharge front splitting by ionization seed profiling," *Physics of Plasmas*, Vol. 26, No. 2, 2019, p. 023513.

[38] Pancheshnyi, S., "Role of electronegative gas admixtures in streamer start, propagation and branching phenomena," *Plasma Sources Science and Technology*, Vol. 14, No. 4, 2005, p. 645.

[39] Pancheshnyi, S., Biagi, S., Bordage, M., Hagelaar, G., Morgan, W., Phelps, A., and Pitchford, L., "The LXCat project: Electron scattering cross sections and swarm parameters for low temperature plasma modeling," Vol. 398, 2012, pp. 148–153.

[40] Bisetti, F., and El Morsli, M., "Calculation and analysis of the mobility and diffusion coefficient of thermal electrons in methane/air premixed flames," *Combustion and flame*, Vol. 159, No. 12, 2012, pp. 3518–3521.